
Study of Response of Extreme Meso-Scale Field-Aligned Current to Interplanetary Magnetic Field Components B_x , B_y and B_z During Geomagnetic Storm

Adero Ochieng Awuor^{1, *}, Paul Baki¹, Olwendo Joseph², Pierre Cilliers³, Pieter Kotze³

¹Department of Physics and Space Science, Technical University of Kenya, Nairobi, Kenya

²Department of Mathematics and Physical Sciences, Pwani University, Mombasa, Kenya

³South Africa National Space Agency, SANSA Space Center, Hermanus, South Africa

Email address:

aderoconstant@gmail.com (A. O. Awuor)

*Corresponding author

To cite this article:

Adero Ochieng Awuor, Paul Baki, Joseph Olwendo, Pierre Cilliers, Pieter Kotze. Study of Response of Extreme Meso-Scale Field-Aligned Current to Interplanetary Magnetic Field Components B_x , B_y and B_z During Geomagnetic Storm. *International Journal of Astrophysics and Space Science*. Vol. 7, No. 1, 2019, pp. 1-11. doi: 10.11648/j.ijass.20190701.11

Received: October 6, 2018; **Accepted:** November 26, 2018; **Published:** August 6, 2019

Abstract: The influence of IMF components on meso-scale field-aligned currents (FACs) is investigated with an aim to establish how different IMF components influence the occurrence and distribution of FACs. The field-aligned currents (FACs) are calculated from the curl of the Ampere's law to the magnetic field recorded by CHAMP satellite during 24 major geomagnetic storms. To determine the field-aligned currents at extreme mesoscale range $\sim 150 - 250$ km, a low-pass filter to FACs with a cutoff period of 20s is applied. The peak-to-peak amplitude of FAC density, with the maximum difference $\leq 3^0$ MLAT, is determined and used to define the FAC range. The results indicate high occurrence of FACs centered about IMF ≈ 0 , for large values of Dst. The magnitude of FACs is in general affected by all the three IMF components, alongside other ionospheric factors such as solar wind speed and density. Magnetic reconnection, under $-B_z$ is a major FACs drivers and is significant in the dayside northern hemisphere. The reconnection is not symmetric in both hemispheres. We find a possible electrodynamic similarity between the dayside northern hemisphere and nightside southern hemisphere, prominent along B_x when B_z is negative. This interesting observation can further be investigated.

Keywords: Auroral Ionosphere, High-latitude Current Systems, Magnetosphere-ionosphere Coupling

1. Introduction

A number of systems of global-scale electrical currents are generated in the near-Earth environments due to the interaction between the solar wind and interplanetary magnetic field. One of such currents is the field-aligned currents (FACs), commonly referred to as Birkeland currents after he first suggested their existence in the upper atmosphere in 1908. This current system plays a role in coupling the energy from the magnetosphere to the high latitude conducting ionospheres. This coupling can lead to magnetospheric perturbations and currents which have been shown to be the cause of various devastating effects on Earth's atmosphere, such as, geomagnetically induced

currents (GICs) on power grids, railways, and other long-distance conducting structures [12]. The dynamics of the high-latitude thermosphere is greatly affected by the energy input from the solar wind via Joule heating and particle precipitation [21, 30]. Further, Joule heating of the thermosphere can have undesired effects on satellites in low Earth orbits [7]. These effects result from large currents, totaling approximately 4 MA for typical solar wind and IMF conditions and increasing as more extreme driving occurs [34]. Thus, a better understanding of the FAC distribution under various geomagnetic conditions and IMF orientations is important for understanding energy transfer in the magnetosphere-ionosphere system. The IMF B_y component significantly changes the patterns of FACs in both the ionosphere and the magnetosphere [11]. The B_y deflections

has been hypothesized to be due to field-aligned currents (FACs) [28]. The effect of polarity of IMF B_y on the FACs topology is reversed in the southern hemisphere due to the antisymmetry of the reconnection site with respect to the noon-midnight meridian [10].

Four types of FACs are known to exist, e.g., Region 1 (R1), Region 2 (R2), northward IMF B_z (NBZ), and IMF B_y modulated (DPY) FACs [16, 17]. R1 FACs flow into the ionosphere in the morning sector and out of the ionosphere in the evening sector, and R2 FACs are located equatorward of the R1 FACs with opposite polarities. For northward IMF B_z , NBZ FACs dominate in the polar cap poleward of R1 FACs [17]. This current system, NBZ FACs, have been interpreted in terms of the antiparallel reconnection on field lines tailward of the dayside cusp [17, 31, 32]. When IMF B_y becomes dominant DPY FACs form around the noon sector while positive B_y , in the northern hemisphere results in upward field-aligned current located poleward of the downward current, and vice versa in the southern hemisphere [16, 2]. The poleward part of DPY currents could be associated with the plasma mantle/cusp precipitation, while the equatorward part is an intrusion of dawnside ($B_y > 0$) or duskside ($B_y < 0$) R1 currents [e.g., 8, 35]. The high-latitude ionospheric convection pattern strongly depends on the orientation of IMF [13]. Normally, for southward IMF two-cell convection flow pattern exists, while for northward IMF four-cell flow pattern emerges due to high-latitude reconnection. IMF B_y will distort the convection map and cause dawn-dusk and interhemispheric asymmetries. The locations of the auroral oval and its activity have been found to strongly depend on the IMF configuration [14]. High auroral power is observed for all negative IMF components [29]. A brighter dayside aurora has also been observed for $B_x < 0$ than for $B_x > 0$ during southward IMF, while the nightside aurora brightness is less dependent on IMF B_x , and the duskside auroral brightness for northward IMF is not so much brighter for $B_x < 0$ than for $B_x > 0$ [36].

The overall response of both the ionospheric convection and field-aligned current distribution to IMF B_z , B_x and B_y has been established. However, the mutual relationship of these components has not been comprehensively examined. The relationship would, for instance, help us understand the mapping of the field-aligned currents from the ionosphere to the magnetosphere. In this study, we will examine the effect of IMF B_x , B_y , and B_z on the ionospheric distribution of FACs by defining a new parameter called FAC range. We define FAC range as peak-to-peak amplitude of FAC density, filtered by a 20s low-pass filter. The location of maximum and minimum peaks is determined by the magnetic latitude (MLAT), with the maximum difference $\leq 3^\circ$ MLAT, alongside the corresponding magnetic local time (MLT) and universal time (UT). The satellite passes with the peaks which are far apart ($>3^\circ$ MLAT) are discarded. This was done to avoid using peaks in different MLT sectors. The FAC range comprises R0, R1 and R2 FACs.

The paper is organized as follows; the data set and methodology are described in section 2. The results are

presented in section 3 while section 4 outlines the discussions. Finally, the conclusion is given in section 5.

2. Data Set and Methodology

2.1. CHAMP Satellite Data

The geoscientific satellite CHAMP was launched on 15 July 2000 into a near circular, near-polar orbit (87.3° inclination) [23, 25]. With initial altitude at 456 km the orbit decayed to about 350 km after 5 years. The orbital plane precesses at rate of 1 h in local time (LT) per 11 days, thus covering all local times within 131 days. The data used here are the vector magnetic field measurements of the Fluxgate Magnetometer (FGM). FGM instrument delivers vector field readings at a rate of 50 Hz. The satellite data used in this study are the pre-processed (level 2) fluxgate magnetometer vector data from CHAMP in sensor frame (product identifier CH-ME-2-FGM-FGM), which has been down sampled to 1.0 Hz.

2.2. Geomagnetic and OMNI IMF/Solar Wind Data

The Dst, IMF B_z (in GSM coordinates) and solar wind dynamic pressure are taken from NASA/Goddard Space Flight Center's (GSFC's) OMNI data set through the OMNIWeb interface. The OMNI data set provides time series of solar wind parameters propagated to their impact on the bowshock [24]. The solar wind data has been time shifted for 15 min to take into account the solar wind propagation through the magnetosheath from the bow shock nose to the magnetopause [5].

2.3. Field-Aligned Currents Density Calculation

The FAC density is determined according to Ampere's law from the vector magnetic field data by solving the curl-B, that is, $j_z = \frac{1}{\mu_0} \left(\frac{\partial B_y}{\partial x} - \frac{\partial B_x}{\partial y} \right)$ where μ_0 is the vacuum permeability, B_x and B_y are the transverse magnetic field deflections caused by the currents. We have assumed that FACs is infinite sheets aligned with the mean location of the auroral oval [33]. Since we do not have multipoint measurements, we convert spatial gradients into temporal variations by considering the velocity under the assumption of the stationary of the current during the time of satellite passage. After discrete sampling is introduced, we obtain $j_z = \frac{1}{\mu_0} \frac{1}{v_x} \frac{\partial B_y}{\partial t}$ where v_x is the velocity perpendicular to the current sheet and B_y is the magnetic deflection component parallel to the sheet [22].

3. Observations

3.1. IMF-FAC Range Variation in Different MLT Sectors

The Figures 1-8 show the variations of FAC range with IMF B_x , B_y and B_z components. The data are classified according to the geomagnetic activity levels and MLT sectors; dayside (0800-1600 MLT), nightside (2000-0400

MLT), dawnside (0500-0700 MLT) and duskside (1700-1900 MLT). We however take note of relatively limited number of data points for some MLT sectors, which could lead to uncertainties in the interpretations.

From left to right, the panels in Figures 1-8 correspond to IMF B_x , B_y and B_z while from top to bottom, we have dayside, nightside, dawnside and duskside sectors respectively. Indeed, the IMF B_x and B_y component affect

both dayside and nightside Polar Regions. The increase of FAC range magnitude corresponded fairly well to an increasing $|B_z|$ during southward IMF, while the magnitude remained fairly constant regardless of $|B_z|$ during northward IMF, clearly seen on the nightside MLT sector. The other IMF components, on the hand, did not show, in general, the increasing FAC range magnitude with increasing IMF.

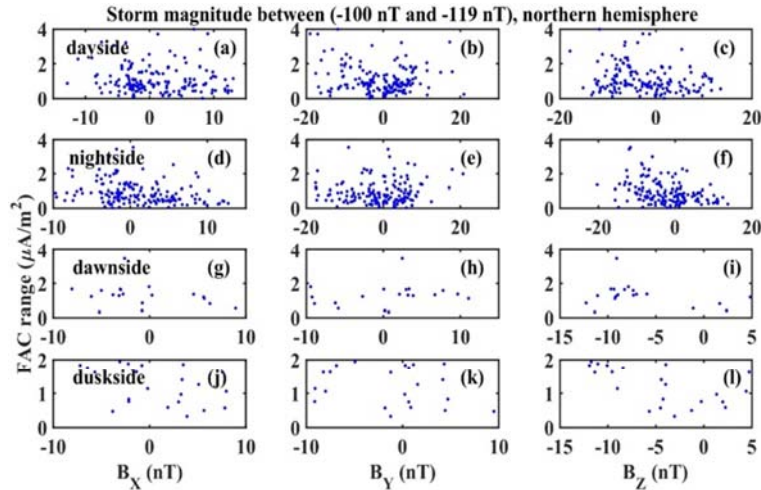


Figure 1. FAC range against various IMF components. Panels a, b and c (dayside), d, e and f (nightside), g, h and i (dawnside) and j, k and l (duskside) in the northern hemisphere. The Dst value between $-119 \leq Dst \leq -100$.

The distribution of FAC range varied differently in all MLT sectors for different IMF components, depending of the negative and positive deflection of the components. Higher FAC range occurrence is exhibited during positive IMF B_x than during negative IMF B_x during the dayside MLT sector and the reverse is observed in the nightside. For the IMF B_y component, higher occurrence of FAC range is observed when the component is negatively deflecting than during positive deflecting. The reverse is observed during the dawn MLT sector. Figure 1 (c and f panels) show IMF B_z , as expected, higher occurrence of FAC range with larger densities is observed during the negative deflection than during the positive deflection. The occurrence of FAC range

is also higher during the dayside MLT sector than the rest of other sectors.

The magnitude of FAC range density increased significantly, possibly responding to the increase in storm magnitude. The increase is more pronounced during the dayside (Figure 2, a-c) MLT sectors. High FAC range occurrence is observed during the negative IMF B_x in all MLT sectors while for IMF B_y the distribution is almost symmetrical about IMF $B_y \approx 0$, but with high magnitudes of FAC range during the negative IMF B_y . The response of FAC range distribution observed during the negative IMF B_z is consistent throughout the MLT sectors.

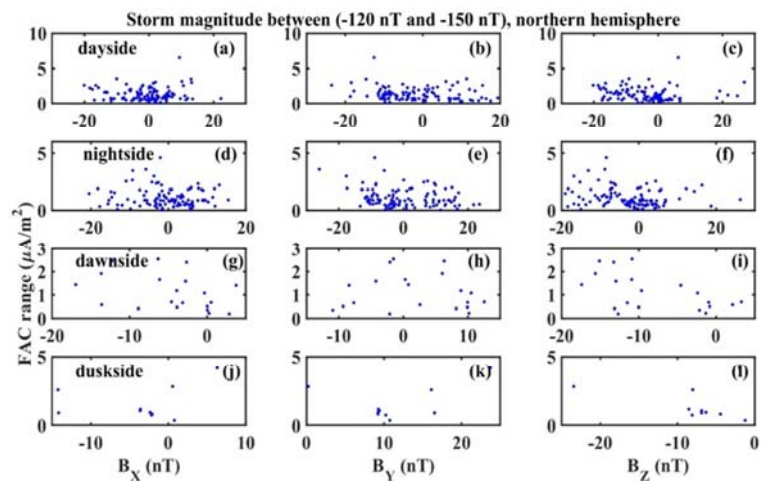


Figure 2. Same as Figure 1 for Dst value between $-150 \leq Dst \leq -120$.

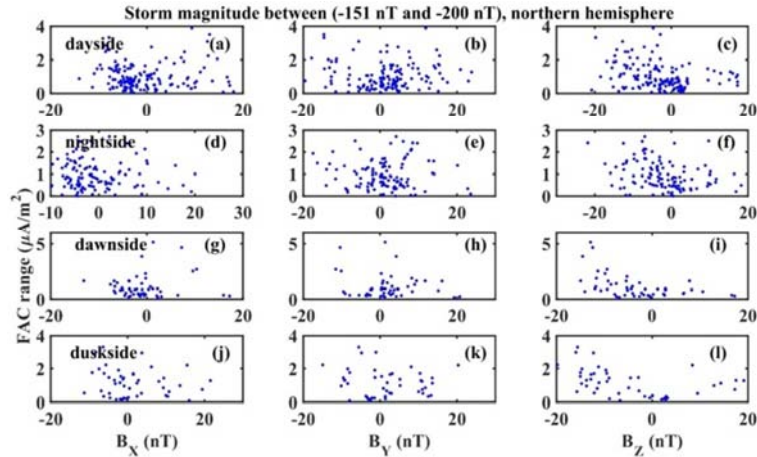


Figure 3. Same as Figure 1 for Dst value between $-200 \leq Dst \leq -151$.

The magnitude of FAC range did not respond significantly to the decrease in the storm main phase ($-151 \text{ nT} \leq Dst \leq -200 \text{ nT}$). The distribution of FAC range is however showing meaningful differences in different MLT sectors. While during the dayside, the occurrence of FAC range is higher for negative deflection of IMF B_X (Figure 3a) and IMF

B_Z (Figure 3c) than during the positive deflections in both cases, the IMF B_Y (Figure 3b) is centered about IMF $B_Y \approx \pm 5 \text{ nT}$. The nightside MLT sector exhibited the same trend. Both dawnside and duskside MLT sectors showed negative deflections of IMF components to favor the occurrence of the FAC range compared to positive deflection.

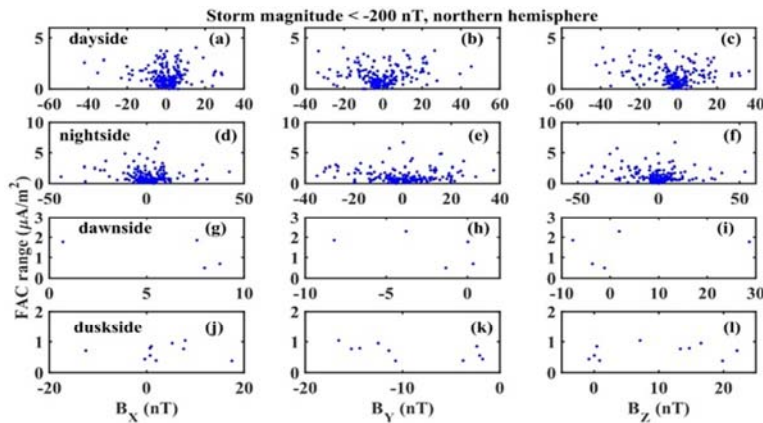


Figure 4. Same as Figure 1 for Dst value $< -200 \text{ nT}$.

Figure 4, panels (d-f), show significant increase in the FAC range magnitude. The most remarkable difference is observed during the dayside MLT sector, panels (a-c), where the distribution of FAC range is almost symmetrical

about $-10 \text{ nT} \leq IMF \leq 10 \text{ nT}$. The FAC range intensities are stronger for large positive and negative values of the B_Z (Figure 4, c and f).

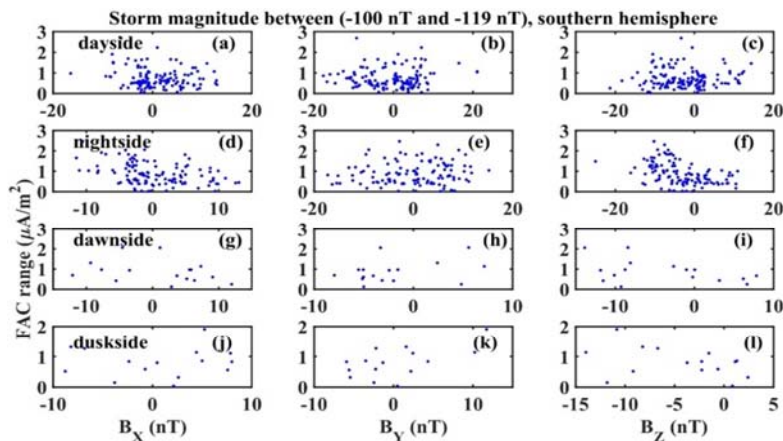


Figure 5. Same as Figure 1 in the southern hemisphere.

There is less occurrence of FAC range in the southern hemisphere compared to similar conditions in the northern hemisphere (Figure 1) with the FAC range distribution about the $-10nT \leq IMF \leq 10nT$. This could imply asymmetry in reconnection in southern and northern hemispheres. Higher FAC range occurrence is exhibited during positive IMF B_x than during negative IMF B_x during the dayside MLT sector and the reverse is observed in the nightside. For the IMF B_y component,

higher occurrence of FAC range is observed when the component is negatively deflecting than during positive deflecting. The reverse is observed during the dawn MLT sector. Figure 1(c and f panels) show IMF B_z , as expected, higher occurrence of FAC range with larger densities is observed during the negative deflection than during the positive deflection. The occurrence of FAC range is also higher during the dayside MLT sector than the rest of other sectors.

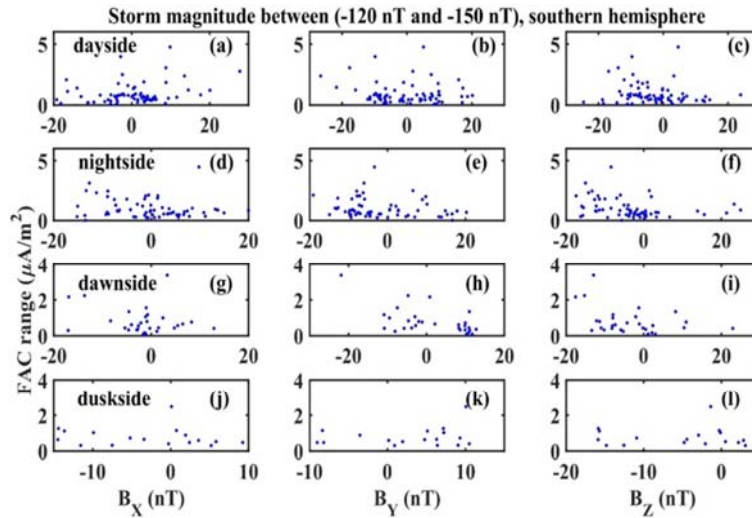


Figure 6. Same as Figure 2 in the southern hemisphere.

Figure 6 shows less occurrence of FAC range in all MLT sectors, with higher magnitudes and distributions during negative IMF B_z component compare to during positive IMF B_z . The IMF B_y component exhibited a roughly symmetric distribution about IMF ≈ 0 , spreading wider during the

dayside and nightside MLT sectors compared to dawn-dusk sectors. The IMF B_x component had dayside FAC range distribution and magnitude responding to positive IMF B_x compared to negative IMF B_x while the reverse is observed during the nightside MLT sector (Figure 6d).

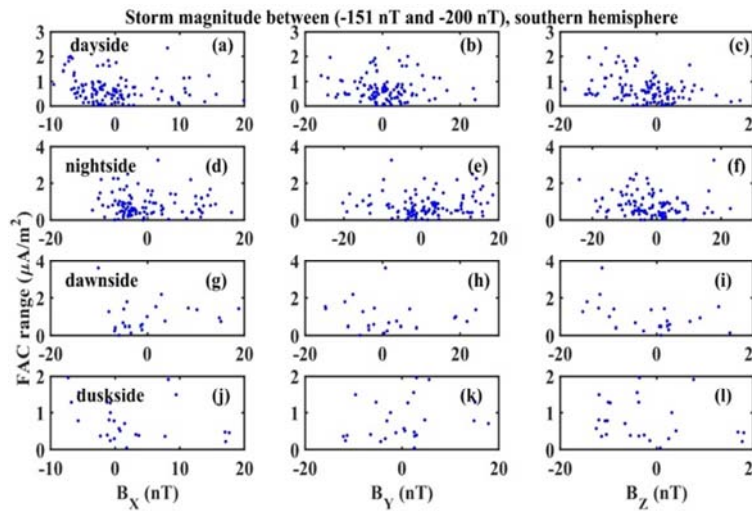


Figure 7. Same as Figure 3 in the southern hemisphere.

The occurrence of FAC range is evidently higher during the $B_x < 0$, in all MLT sectors. For IMF B_y , the dayside MLT sector (Figure 7b) showed, to some extent, symmetrical distribution of FAC range for both negative and positive deflections. The same is observed during the duskside MLT sector (Figure 7k). During the nightside MLT sector, the

distribution of FAC range was evidently high for $B_y > 0$ (Figure 7e) and the reverse observation is made for the dawnside MLT sector (Figure 7h). The IMF B_z components, as expected had higher distribution of FAC range during $B_z < 0$ as compared to $B_z > 0$, in all MLT sectors, however with high occurrence during the dayside MLT sector (Figure 7c).

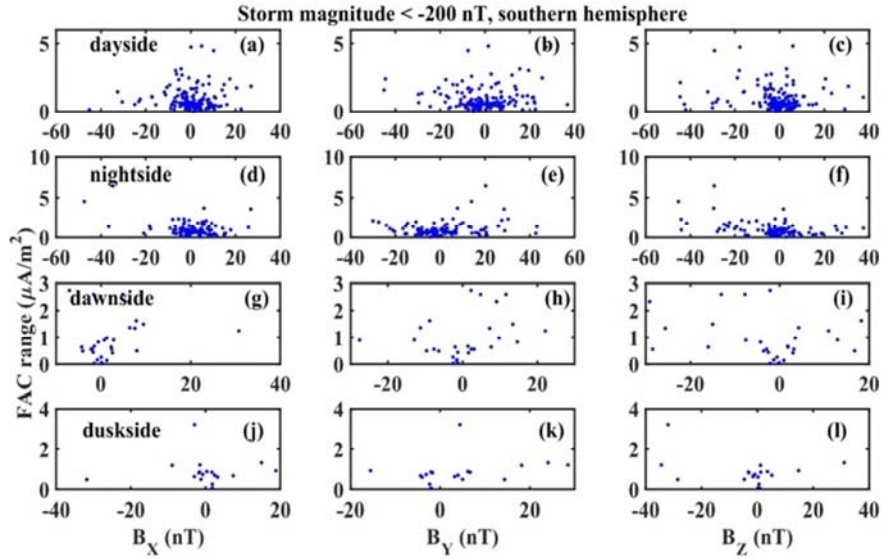


Figure 8. Same as Figure 4 in the southern hemisphere.

The distribution of FAC range tends to concentrate between $-10 \leq IMF \leq 10$ for dayside and nightside MLT sectors. The same trend is exhibited in dawnside and duskside sectors though with less symmetric distribution about the $IMF \approx 0$. The dayside MLT sector still exhibited higher occurrence of FAC range compared to nightside sector. The magnitude of FAC range did not vary much correspondingly to the increase in Dst.

3.2. Day-night FAC Range Dependence on the Orientation of IMF

In this section, we investigate the FAC range cases in IMF

B_X - B_Z and IMF B_Y - B_Z planes in different orientations (positive and negative deflections) in northern and southern hemispheres. The position of the circle is determined by the corresponding values of the IMF components while the size of the circle represents the magnitude of the FAC range. The IMF orientations are categorized as $(B_Z > 0, B_X > 0)$, $(B_Z < 0, B_X < 0)$, $(B_Z > 0, B_X < 0)$ and $(B_Z < 0, B_X > 0)$ for IMF B_X - B_Z plane and the same conditions are considered for IMF B_Y - B_Z plane.

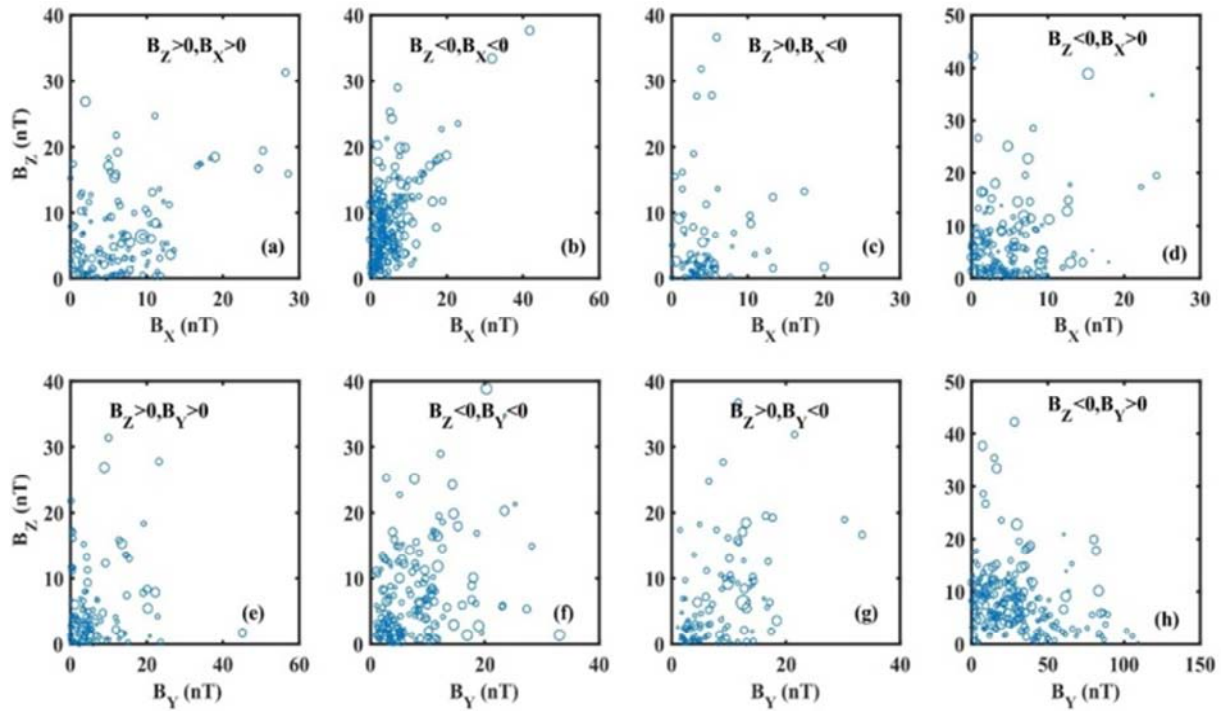


Figure 9. Relationship between the IMF B_X , IMF B_Y and B_Z with the FAC range. Area of the circle represents the magnitude of FAC range, dayside northern hemisphere.

From the plots, some general observations could be made such as for IMF $B_Z < 0$ and $B_Y > 0$, the occurrence of FAC

range is prevalent along the IMF B_Z compared to IMF B_Y in all cases (Figure 9h, 10h, 11h and 12h). This indicates the dominance of negative IMF B_Z over positive IMF B_Y . The positive IMF B_Z component was dominant over negative B_X in the northern hemisphere (Figures 9c and 10c), with more FAC range cases occurring along the IMF $B_Z > 0$. This is not the case in the corresponding day-night sectors in the southern hemisphere (Figures 11c and 12c). A nearly linear relationship between IMF $+B_Z$ and IMF $+B_X$ is observed in both hemispheres, with a clear linear dependence in the northern hemisphere night sector (Figure 10 a, b) and southern day sector (Figure 11a, b), indicating a possible electrodynamic similarities between nightside northern hemisphere and dayside southern hemisphere. The similarity can be further investigated. The FAC range magnitudes are stronger for large $-B_Z$ compared to large $+B_Z$. FAC range occurrence and magnitude seem to favor large values of $|IMF B_Y|$, prominent in northern hemisphere than in southern hemisphere whenever IMF $B_Z < 0$. The north-south hemispheres asymmetry is observed in the IMF B_X component. The northern hemisphere dayside (Figure 9a) FAC occurrence showed a similar behaviour as the southern nightside FAC cases (Figure 12a). Similar observations are

made between northern hemisphere nightside (Figure 10a) and the dayside FAC range occurrence in the southern hemisphere (Figure 11a).

High occurrence of FAC range is observed for small values of IMF components. For $B_Z > 0, B_X > 0$, large FAC range density occur when IMF B_Z is small and $B_X \sim 10$ nT (Figure 9a). The distribution of FAC range favored the large values of B_X , corresponding to large values of B_Z . For southward IMF B_Z and negative IMF B_X (Figure 9b), the large FAC range density occurs for large IMF B_Z with more cases of FAC range occurring for small negative IMF B_X . Figure 9c compares FAC range cases for positive IMF B_Z and negative IMF B_X . Few cases of FAC range is exhibited under this condition, with large FAC range density occurring for small B_Z and B_X . The large FAC range occurred during large negative IMF B_Z (Figure 9d). While comparing the FAC range occurrence with different orientations of IMF B_Z and IMF B_Y , the FAC range cases are more prevalent during IMF $B_Z < 0$, (Figure 9f and 9h). During IMF $B_Z > 0$, larger FAC range occurred during negative B_Y (Figure 9g) compared to positive B_Y , (Figure 9e). However, the FAC ranges with large densities tend to occur in the large $|IMF B_Y|$ and small $|IMF B_Z|$ region in all cases in IMF B_Z - B_Y plane.

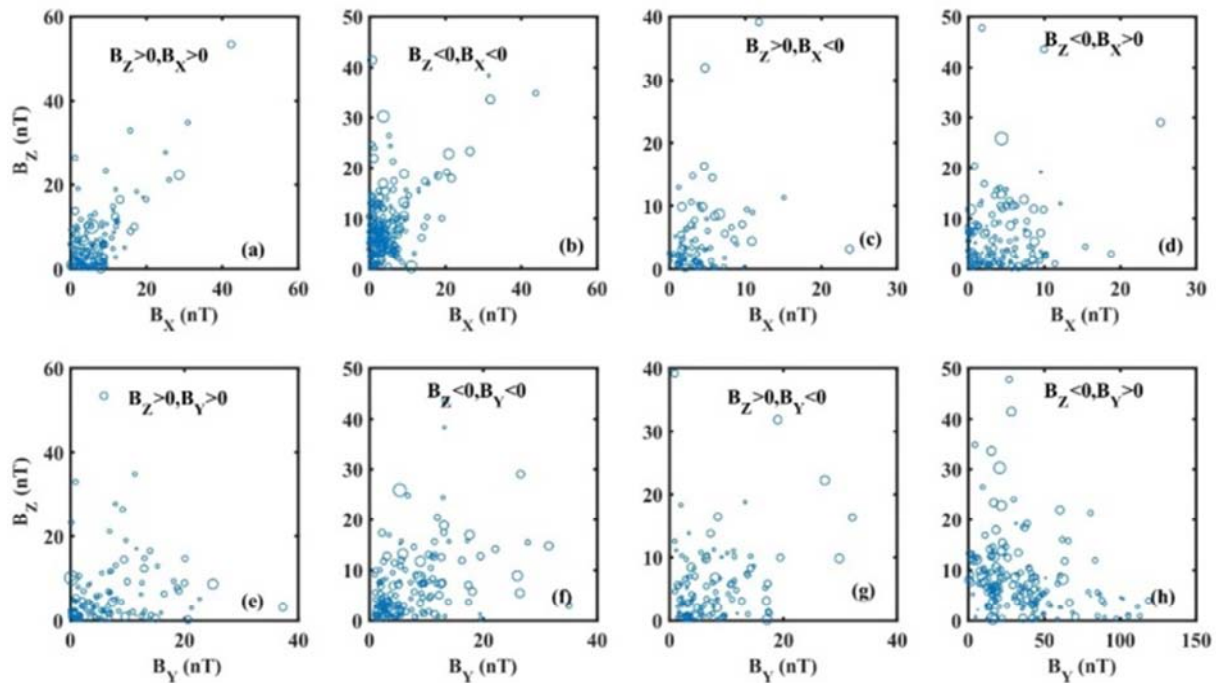


Figure 10. Same as Figure 9 for nightside northern hemisphere.

The nightside FAC range seemingly enjoy a linear relationship in the IMF B_Z - B_X plane, when both components are positive (Figure 10a). Large FAC range densities are however observed for small IMF B_Z and B_X . When both components are negative (Figure 10b), the negative IMF B_Z components dominates in terms of FAC range occurrence and also large values of FAC range are seen during large values of negative IMF B_Z . Interchanging the directions of the IMF components, with positive IMF B_Z and negative IMF B_X (Figure 10c) leave no components preferred for the

occurrence of FAC range. The large density FAC range occur for the small values of the IMF components in this condition. For the case of negative IMF B_Z and $B_X > 0$ (Figure 10d), more FAC range occurred along IMF B_Z . Large FAC range density are observed during large values of IMF $B_Z < 0$ and small IMF $B_X > 0$. In the IMF B_Z - B_Y plane, the occurrence of FAC range was prevalent in B_Y component than along B_Z except for IMF $B_Z < 0$ and $B_Y > 0$ (Figure 10h). Large FAC range density occurred during large IMF B_Z and small IMF B_Y whenever $B_Z < 0$ (Figure 10f and 10h).

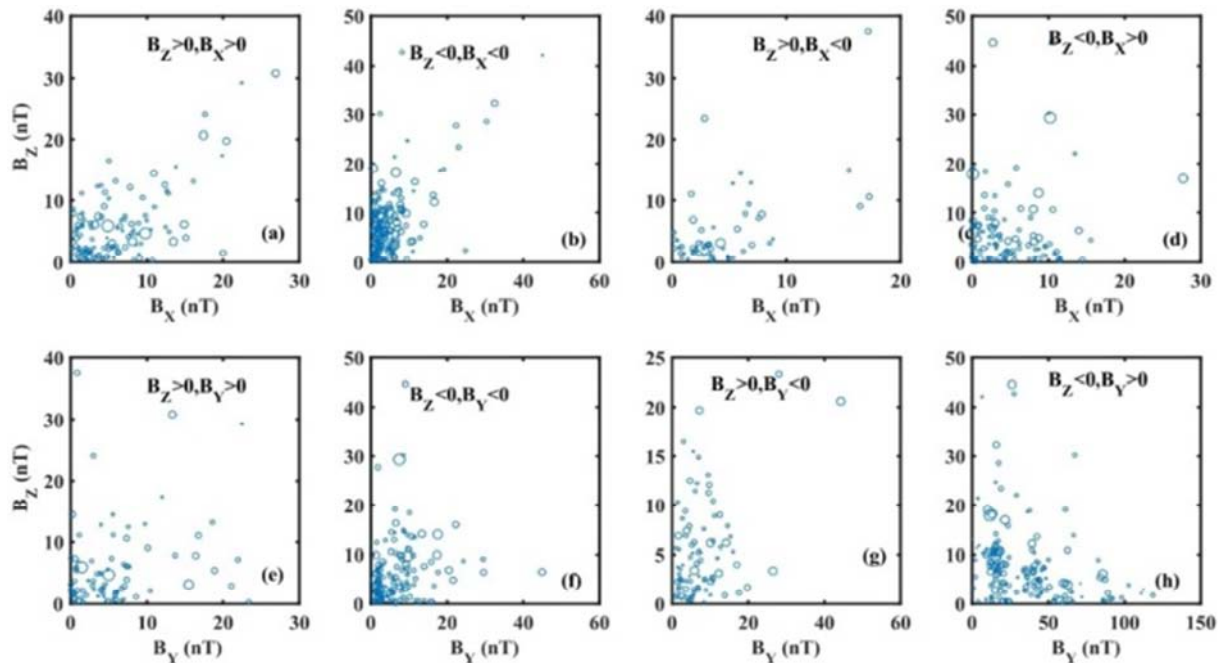


Figure 11. Same as Figure 9 for dayside southern hemisphere.

The possible linear relationship between the IMF B_Z - B_X plane FAC range when both components are possible (Figure 11a) while the larger FAC range are observed for small values of IMF B_Z and B_X . Similar observations are exhibited when IMF B_Z and B_X are negative (Figure 11b). For IMF $B_Z > 0$ and $B_X < 0$, few cases of FAC range are observed with the large density FAC range occurring when IMF B_Z is very small

(Figure 11c). In Figure 11d, large values of FAC range density are observed during large values of IMF B_Z . In the IMF B_Z - B_Y plane, except for both positive IMF B_Z and B_Y (Figure 11e) where large values occurred for small values of IMF B_Z and B_Y , Figure 11f, g and h, shows dominant occurrence of FAC range along the IMF B_Z component. Large values of FAC range are observed when IMF B_Y is very small.

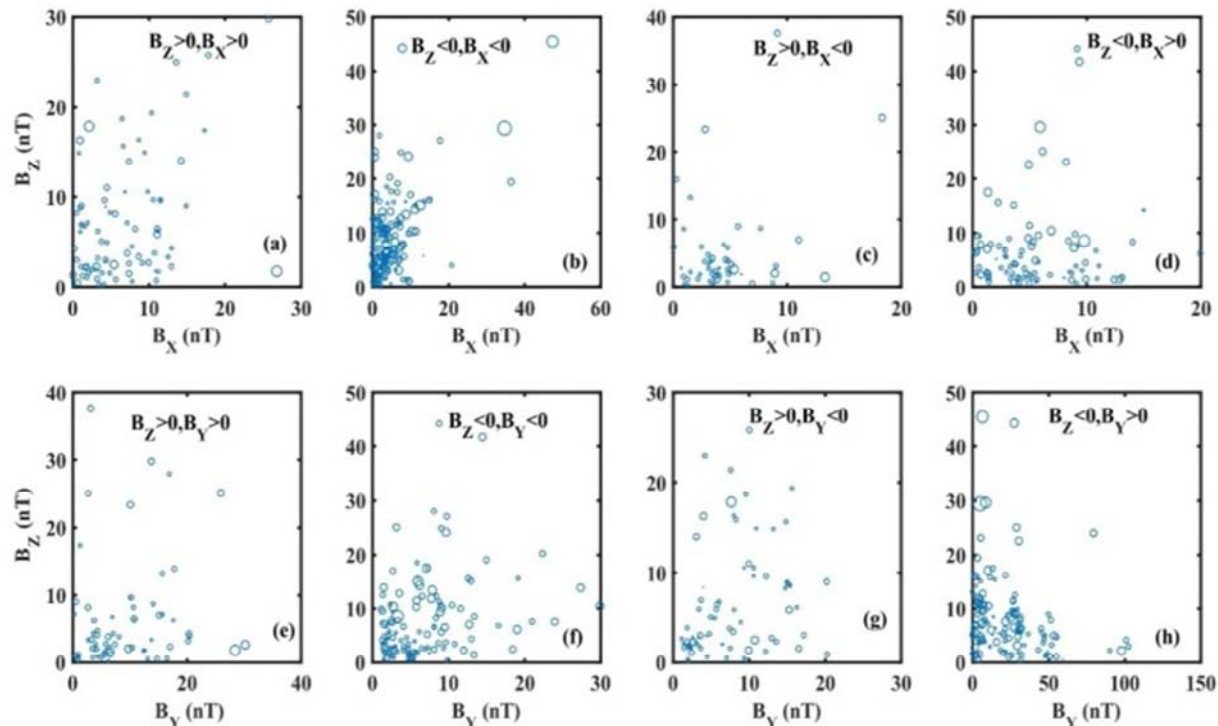


Figure 12. Same as Figure 9 for nightside southern hemisphere.

The nightside southern hemisphere, Figure 12, showed

occurrence of large FAC range values in both components for

the both large values of IMF B_Z and B_X positive (Figure 12a) and IMF B_Z and B_X negative (Figure 12b). For $B_Z > 0$ and $B_X < 0$ large FAC range values are observed for large values of IMF B_X (Figure 12c). For IMF $B_Z < 0$ and IMF $B_X > 0$, the large values of FAC range occurred during large values of IMF B_Z . The IMF B_Z - B_Y plane had large values of FAC range when B_Y was large and small B_Z (Figure 12e) while large values of FAC range are observed for large values of IMF B_Z and small magnitude of IMF B_Y for IMF $B_Z < 0$, IMF $B_Y > 0$ (Figure 12h).

4. Discussions

Interplanetary magnetic field (IMF) influences on the occurrence of large-scale FACs has been long recognized [31, 19, 1]. The IMF influence on the FACs is however not from only a single IMF component but a contribution from all the IMF components. For instance, it has been found that in the polar region the distribution, scale, and magnitude of the Joule heating region, and the corresponding FACs, are controlled mainly by the IMF clock angle, which is determined by the B_Y and B_Z components of the IMF [20]. The occurrences and patterns of the high-latitude field-aligned currents (FACs) observed in Figures 1-12 are an indication of the solar wind-magnetosphere-ionosphere coupling. Using geomagnetic data from CHAMP satellite, during geomagnetic storm, the study has investigated the occurrences and intensifications of FAC range for different interplanetary magnetic field (IMF) orientations and amplitudes for 24 different storms. The intensification of FACs manifested in large magnitudes of FAC range during southward IMF B_Z compared to northward IMF B_Z (Figures 1-8, IMF B_Z column) indicating that the magnetopause is closer to Earth under southward IMF than under northward IMF B_Z . Similar observations are made in IMF planes, whenever IMF $B_Z < 0$, (Figures 9-12). The dayside sector has exhibited high occurrences of FAC range indicating significant influence of dayside magnetic reconnection. Magnetic reconnection has also been alluded to as the main driver for strong FACs originating from magnetopause boundary during the southward IMF [15, 4]. This implies that the merging between the IMF and Earth's magnetic field creates open field lines that are transported tailward by the magnetosheath flow in accordance to [6]. During IMF $-B_Z$, magnetic flux is removed from the dayside and added into the tail flux tubes. The open flux is then closed by subsequent reconnection in the magnetotail and returned to the dayside by sunward convection. The magnetotail reconnection explains the observed nightside high occurrence of FAC range cases (Figures 1-8, second row).

The influence of the level of geomagnetic activity on FAC range is evident on both hemispheres. With the increase in the activity level ($Dst < -200$ nT), the FAC range magnitude remains fairly constant for $|IMF|$ (Figures 4 and 8). The observed enhanced fluctuations are consistent with the enhanced FACs reported by [3].

For geomagnetic activity ≥ -200 nT, Figures 1-3, northern

hemisphere and Figures 5-7, southern hemisphere, the occurrence and magnitude of FAC range fairly depended on the orientation of IMF. This concurs with the observation that high-latitude ionospheric convection pattern strongly depends on the orientation of IMF [13]. The occurrences and intensity of FAC range is higher during the negative deflection of IMF components compared to positive deflection, affirming the observations by [29, 35].

The nightside FAC range showed a clear dependence on IMF B_Z (Figures 1f, 2f, 5f, 6f and 7f), with increasing magnitude of FAC range with increasing IMF $-B_Z$ and a fairly constant FAC range magnitude during IMF $+B_Z$ compared to their dayside counterparts. This apparent dependence on IMF B_Z could be due to the relationship between IMF B_Z and AL index [9]. A similar observation was also made by [18].

The magnitude of FAC range increased, to some extent, with increasing $|IMF B_Y|$ while higher occurrence as observed around $-10 \leq |IMF B_Y| \leq 10$ during both dayside and nightside (Figures 1-8). Figures 9-12 also showed increasing occurrence and magnitude of FAC range cases with increasing $|IMF B_Y|$, whenever $B_Z < 0$. This affirms that IMF B_Y component affects not only the dayside polar region but also the nightside polar region and consistent with the observations by a number of scholars. The influence of IMF B_Y on the FACs near the midnight auroral oval, where the intensity of the currents increases with $|B_Y|$ was observed by [27]. Further, the coherent B_Y -controlled convection exists near the midnight auroral oval when IMF is stable, and when its magnitude is large, and that the distribution of the FACs is associated with B_Y -controlled convection [26]. IMF B_Y component changes the location of the reconnection site on the magnetopause, leading to a number of asymmetric features. On the dayside, finite IMF B_Y shifts the dayside reconnection site from the subsolar point, toward high-latitude flanks, where antiparallel reconnection is dominant.

The north-south asymmetry in the IMF B_X component could be due to the magnetopause reconnection location. For $B_Z < 0$, a positive (negative) B_X might be expected to move the preferred reconnection location northward (southward) along the closed dayside field line. Closed dayside flux may be transferred to open nightside flux and the ionospheric projection would be expected to behave the same way as the southward IMF. For $B_Z > 0$, a positive (negative) B_X is expected to favor open-to-open lobe reconnection in the southern (northern) hemisphere.

5. Conclusion

The higher occurrence of FAC range cases during the dayside sector, with IMF $-B_Z$ is not unusual as these conditions favor dayside reconnections. However, we find a dominant occurrence of FAC range in northern hemispheres compared to southern hemisphere suggesting a possible asymmetry in reconnection sites in southern and northern hemispheres. All the IMF components influence the distribution of FACs.

Although the IMF magnitude affects the magnitude/intensity of FACs, other ionospheric parameters such as solar wind speed and density (not studied here), may also be of great influence. The IMF B_x drives the north-south asymmetry, with the north dayside depicting a similar electrodynamic to the south nightside.

Acknowledgements

The operational support of the CHAMP satellite mission, the World Data Center, Kyoto, the GSFC/SPDF OMNIWeb interface at <http://omniweb.gsfc.nasa.gov>, from where the data used in this study was obtained, are sincerely acknowledged. This work was also supported by the South Africa National Space Agency (SANSA), Technical University of Kenya (TUK) and the National Commission for Science, Technology and Innovation (NACOSTI).

References

- [1] Cheng, Z. W., Shi, J. K., Dunlop, M., & Liu, Z. X. (2013). Influences of the interplanetary magnetic field clock angle and cone angle on the field-aligned currents in the magnetotail. *Geophysical Research Letters*, *40*(20), 5355–5359. <https://doi.org/10.1002/2013GL056737>.
- [2] Clauer, C. R., and E. Friis-Christensen (1988), High-latitude dayside electric fields and currents during strong northward interplanetary magnetic field-Observations and model simulation, *J. Geophys. Res.*, *93*, 2749–2757.
- [3] Coxon, J. C., Milan, S. E., Clausen, L. B. N., Anderson, B. J., and Korth, H. (2014). Journal of Geophysical Research: Space Physics A superposed epoch analysis of the regions 1 and 2 Birkeland currents observed by AMPERE during substorms, 9834–9846. <https://doi.org/10.1002/2014JA020500>. Abstract.
- [4] Cowley, S. W. H. (2000). Magnetosphere-ionosphere interactions: A tutorial review. *Geophysical Monograph Series*, *118*, 91–106. <https://doi.org/10.1029/GM118p0091>.
- [5] Cowley, S., and M. Lockwood (1997), Incoherent scatter radar observations related to magnetospheric dynamics, *Adv. Space Res.*, *20*(4), 873–882, doi: 10.1016/S0273-1177(97)00495.
- [6] Dungey, J. W. (1961). Interplanetary magnetic field and the auroral zones. *Physical Review Letters*, *6*(2), 47.
- [7] Edwards, T. R., D. R. Weimer, W. K. Tobiska, and N. Olsen (2017), Field-aligned current response to solar indices, *J. Geophys. Res. Space Physics*, *122*, 5798–5815, doi: 10.1002/2016JA023563.
- [8] Friis-Christensen, E., Y. Kamide, A. D. Richmond, and S. Matsushita (1985), Interplanetary magnetic field control of high-latitude electric fields and currents determined from Greenland magnetometer data, *J. Geophys. Res.*, *90*, 1325–1338.
- [9] Gjerloev, J., Ohtani, S., Iijima, T., Anderson, B., Slavin, J., and Le, G.: Characteristics of the terrestrial field-aligned current system. In *Annales Geophysicae*, volume 29, pages 1713–1729. Copernicus GmbH, 2011.
- [10] Green, C. L. Waters¹, B. J. Anderson, and H. Korth (2009), Seasonal and interplanetary magnetic field dependence of the field-aligned currents for both Northern and Southern Hemispheres, *Ann. Geophys.*, *27*, 1701–1715.
- [11] Guo and C. Wang (2010), Effect of the dawn-dusk interplanetary magnetic field B_y on the field-aligned current system, *JOURNAL OF GEOPHYSICAL RESEARCH*, VOL. *115*, A01206, doi: 10.1029/2009JA014590, 2010.
- [12] Gummow, R. A. (2002), GIC effects on pipeline corrosion control systems, *J. Atmos. Sol. Terr. Phys.*, *64*, 1755–1764.
- [13] Heelis, R. A., J. D. Winningham, M. Sugiura, and N. C. Maynard (1984), Particle acceleration parallel and perpendicular to the magnetic field observed by DE-2, *J. Geophys. Res.*, *89*, 3893–3902, doi: 10.1029/JA089iA06p03893.
- [14] Holzworth, R. H., and C.-I. Meng (1975), Mathematical representation of the auroral oval, *Geophys. Res. Lett.*, *2*, 377–380, doi: 10.1029/GL002i009p00377.
- [15] Hones, E. (1984). Field-aligned currents near the magnetosphere boundary, in *Magnetospheric Currents*, edited by T. A. Potemra., *AGU, Washington, D. C.*, 171–179. <https://doi.org/10.1029/GM028p0171>.
- [16] Iijima, T., and T. Potemra (1976), Field-aligned currents in the dayside cusp observed by Triad, *J. Geophys. Res.*, *81*, 5971–5979.
- [17] Iijima, T., T. A. Potemra, L. J. Zanetti, and P. F. Bythrow (1984), Large-scale Birke-land currents in the dayside polar region during strongly northward IMF: Anew Birkeland current system, *J. Geophys. Res.*, *89*, 7441–7452.
- [18] Juusola, L., K. Kauristie, O. Amm, and P. Ritter (2009), Statistical dependence of auroral ionospheric currents on solar wind and geomagnetic parameters from 5 years of CHAMP satellite data, *Ann. Geophys.*, *27*, 1005–1017.
- [19] Juusola, L., Milan, S. E., Lester, M., Grocott, A., & M. Imber, S. (2014). Interplanetary magnetic field control of the ionospheric field-aligned current and convection distributions. *Journal of Geophysical Research: Space Physics*, *119*(4), 3130–3149. <https://doi.org/10.1002/2013JA019455>.
- [20] Li, H., Wang, C., & Kan, J. R. (2011). Contribution of the partial ring current to the SYMH index during magnetic storms. *Journal of Geophysical Research: Space Physics*, *116*(11), 1–12. <https://doi.org/10.1029/2011JA016886>.
- [21] Luhr, H., M. Rotter, W. Kohler, P. Ritter, and L. Grunwaldt (2004), Thermospheric up-welling in the cusp region: Evidence from CHAMP observations, *Geophys. Res. Lett.*, *31*, L06805, doi: 10.1029/2003GL019314.
- [22] Luhr, H., Warnecke, J., and Rother, M. K. A.: An algorithm for estimating field aligned currents from single spacecraft magnetic field measurements: A diagnostic tool applied to Freja satellite data, *Geosci. Remote Sens.*, *34*, 1369–1376, 1996.
- [23] Maus, S., M. Rother, C. Stolle, W. Mai, S. Choi, H. Lühr, D. Cooke, and C. Roth (2006), Third generation of the Potsdam Magnetic Model of the Earth (POMME), *Geochem. Geophys. Geosyst.*, *7*, Q07008, doi: 10.1029/2006GC001269.
- [24] Papitashvili, V. O., N. E. Papitashvili, and J. H. King (2000), Solar cycle effects in planetary geomagnetic activity: Analysis of 36-year long OMNI dataset, *Geophys. Res. Lett.*, *27*(17), 2797–2800, doi: 10.1029/2000GL000064.

- [25] Reigber, C., Luhr, H., and Schwintzer, P.: Champ mission status, *Advances in Space Research*, 30: 129–134, 2002.
- [26] Taguchi, S., M. Sugiura, T. Winningham, and J. A. Slavin (1994), By-controlled convection and field-aligned currents near midnight auroral oval for northward interplanetary magnetic field, *J. Geophys. Res.*, 99, 6027–6044.
- [27] Taguchi, S (1992), By-controlled field-aligned currents near midnight auroral oval during northward Interplanetary magnetic field, *J. Geophys. Res.*, 97, 12 231–12 243.
- [28] Sarafopoulos Dimitrios (2016), The Pattern of By Deflections Produced from Field-Aligned Currents Earthward of the Activation Source in the Earth's Magnetosphere, *International Journal of Geosciences*, 479-500.
- [29] Shue, J.-H., P. T. Newell, K. Liou, C.-I. Meng, and S. W. H. Cowley (2002), Interplanetary magnetic field Bx asymmetry effect on auroral brightness, *J. Geophys. Res.*, 107(A8), 1197, doi: 10.1029/2001JA000229.
- [30] Strangeway, R. J., R. E. Ergun, Y.-J. Su, C. W. Carlson, and R. C. Elphic (2005), Factors controlling ionospheric outflows as observed at intermediate altitudes, *J. Geophys. Res.*, 110, A03221, doi: 10.1029/2004JA010829.
- [31] Wang, H., Lühr, H., Ridley, A., Huang, T., and others. (2014). The spatial distribution of region 2 field-aligned currents relative to subauroral polarization stream. *Ann. Geophys.*, 32, 533–542.
- [32] Wang, H., A. J. Ridley, and H. Luhr (2008a), SWMF simulation of field-aligned currents for a varying northward and duskward IMF with nonzero dipole tilt, *Ann. Geophys.*, 26, 1461-1477, doi: 10.5194/angeo-26-1461-2008.
- [33] Wang, H., H. Luhr, and S. Y. Ma (2005), Solar zenith angle and merging electric field control of field-aligned currents: A statistical study of the Southern Hemisphere, *J. Geophys. Res.*, 110, A03306, doi: 10.1029/2004JA010530.
- [34] Weimer, D. R. (2005a), Improved ionospheric electrodynamic models and application to calculating Joule heating rates, *J. Geophys. Res.*, 110, A05306, doi: 10.1029/2004JA010884.
- [35] Wing, S., S.-I. Ohtani, P. T. Newell, T. Higuchi, G. Ueno, and J. M. Weygand (2010), Dayside field-aligned current source regions, *J. Geophys. Res.*, 115, A12215, doi: 10.1029/2010JA015837.
- [36] Yang, Y. F., J. Y. Lu, J.-S. Wang, Z. Peng, and L. Zhou (2013), Influence of interplanetary magnetic field and solar wind on auroral brightness in different regions, *J. Geophys. Res. Space Physics*, 118, 209-217, doi: 10.1029/2012JA0